SI Appendix

figs. S1-S12

Tables S1 and S2

Movies legends S1 – S11

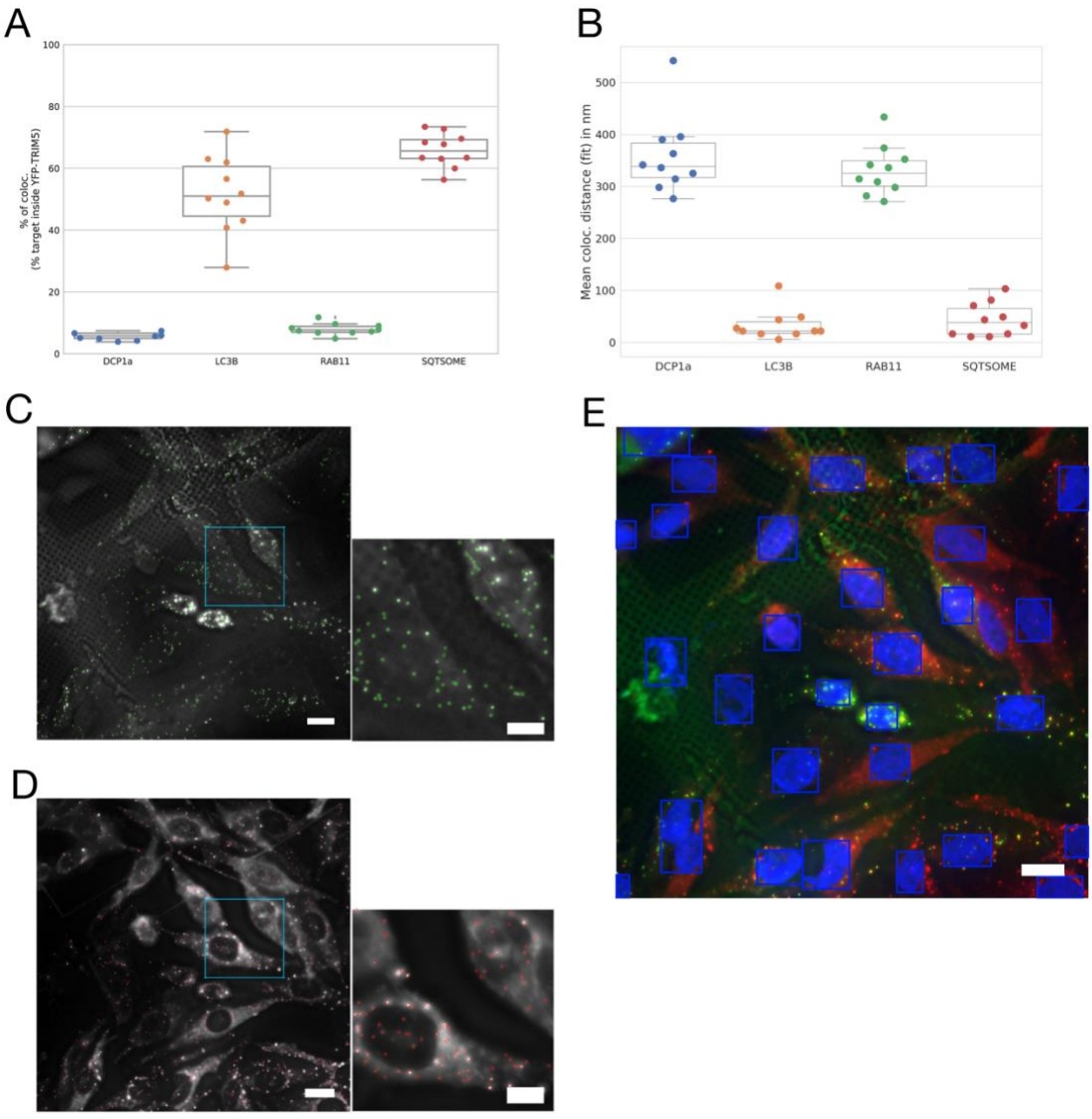

Supplementary figure 1. Carter et al

Figure S1. Spot and cell number detection analysis. Colocalization analysis between YFP-rhTRIM5α and cellular markers. (A) % of colocalization between TRIM5α and the given markers (on the X axis) obtained with object-based colocalization with a distance < 542 nm. DCP1A and RAB11 do not associate with YFP-rhTRIM5α bodies while LC3B and SQSTM1/p62 markers are strongly associated with YFP-rhTRIM5α. **(B)** Mean colocalization distance in colocalization events between TRIM5α and various markers (limit is 5 px = 542 nm). The mean distance for LC3B and SQTSOME colocalization is under the diffraction limit

for the imaging conditions, supporting a strong association. The mean distance for DCP1A and RAB11 colocalization is over the diffraction limit, suggesting that the ~5% colocalization shown in (A) is due to imaging and analysis artifacts. **(C and D)** Spots were detected using Icy (2.0.3) spot detection function. An example is shown with signal in grayscale and dots for detected puncta. Green: YFP-rhTRIM5α **(C)**, red: SQSTM1/p62 **(D)**. **(E)** Numbers of cells were estimated using Icy with HK-means detection of nuclei. Channel overlay (green: YFP-rhTRIM5α, red: SQSTM1/p62, blue: Hoechst) is shown with detected ROIs in blue boxes. Scale bars = 20 μm in overview images and 10 μm in channel views.

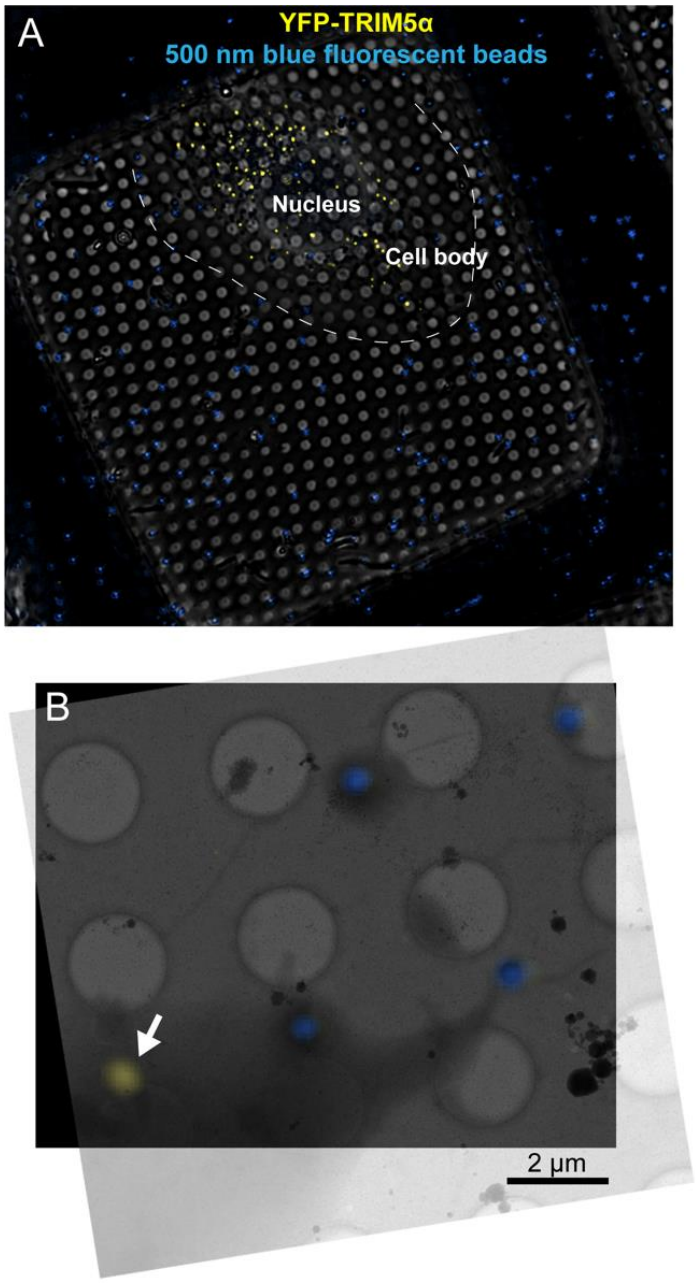

Supplementary figure 2. Carter et al

Figure S2. HeLa cell line 25 exhibits strong YFP-rhTRIM5α fluorescent bodies at 80 K. (A) Deconvolved cryo-LM image (composite of phase contrast and epifluorescence in YFP and DAPI channels) of HeLa cells stably expressing YFP-rhTRIM5α grown on an EM grid with 500 nm blue beads added before freezing. **(B)** Deconvolved epifluorescence image overlaid

on a low-magnification cryo-EM projection image. The white arrow highlights a YFP-rhTRIM5α fluorescent body. Scale bar = 2 μm.

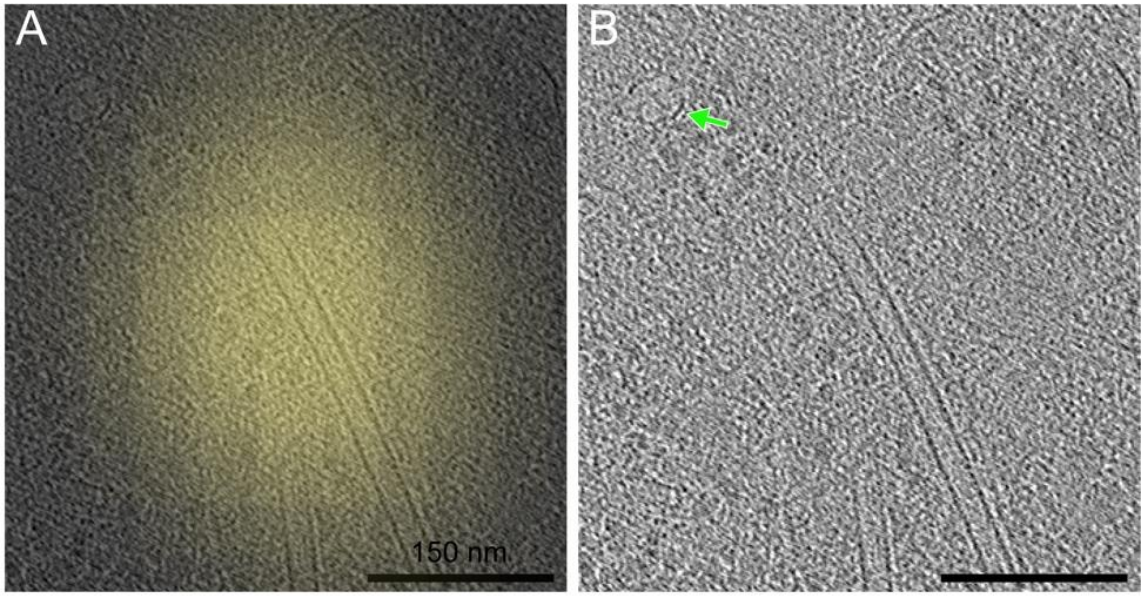

Supplementary figure 3. Carter et al

Figure S3. Cryo-CLEM reveals YFP-rhTRIM5α fluorescent bodies localize near vault complexes. The green arrow highlights a vault complex. Scale bars = 150 nm.

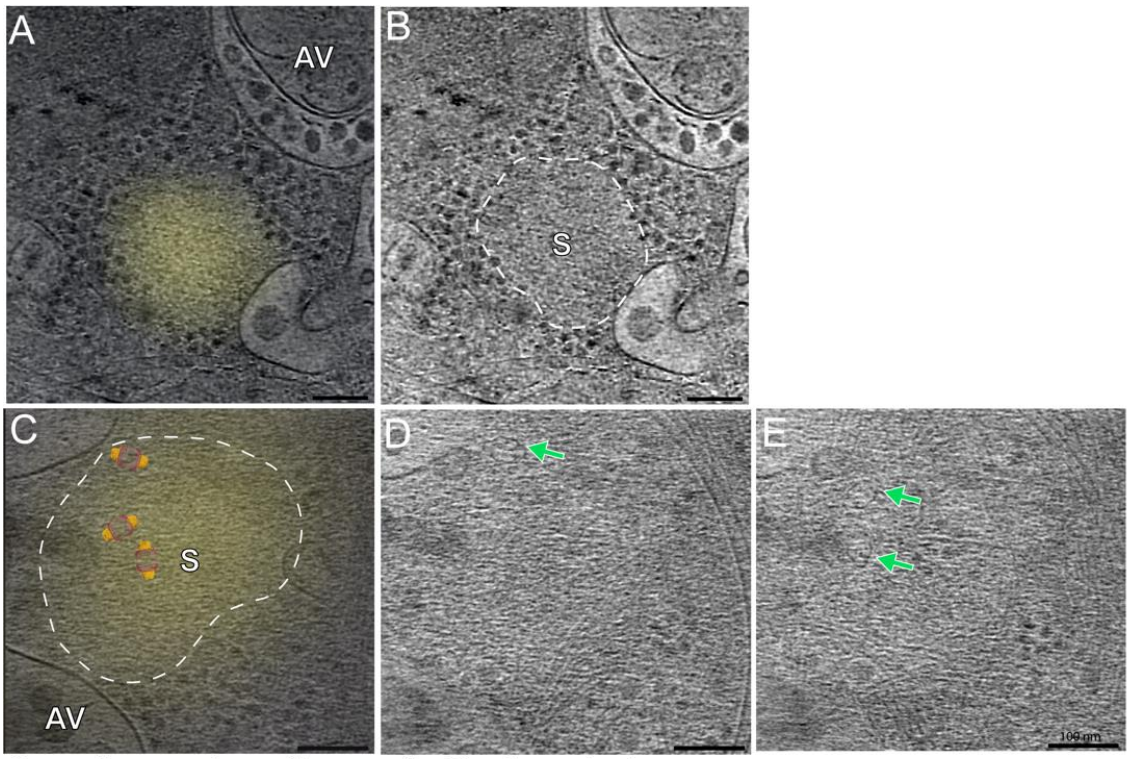

Supplementary figure 4. Carter et al

Figure S4. Cryo-CLEM reveals YFP-rhTRIM5α fluorescent bodies expressed in HeLa cells localize to cytosolic sequestosomes. (A) and (C) Deconvolved epifluorescence images overlaid onto high-magnification cryo-tomogram slices. **(B) and (D)** The cryo-tomographic slice without fluorescence. The border of the sequestosome is highlighted with a white dashed line, and the green arrow highlights a vault complex. **(E)** A different slice of the same region shown in (D) highlighting additional vault complexes. In (C) the locations of the three vaults seen in (D) and (E) are overlaid with crystal structures (PDB:4V60) [1]. Scale bars = 100 nm.

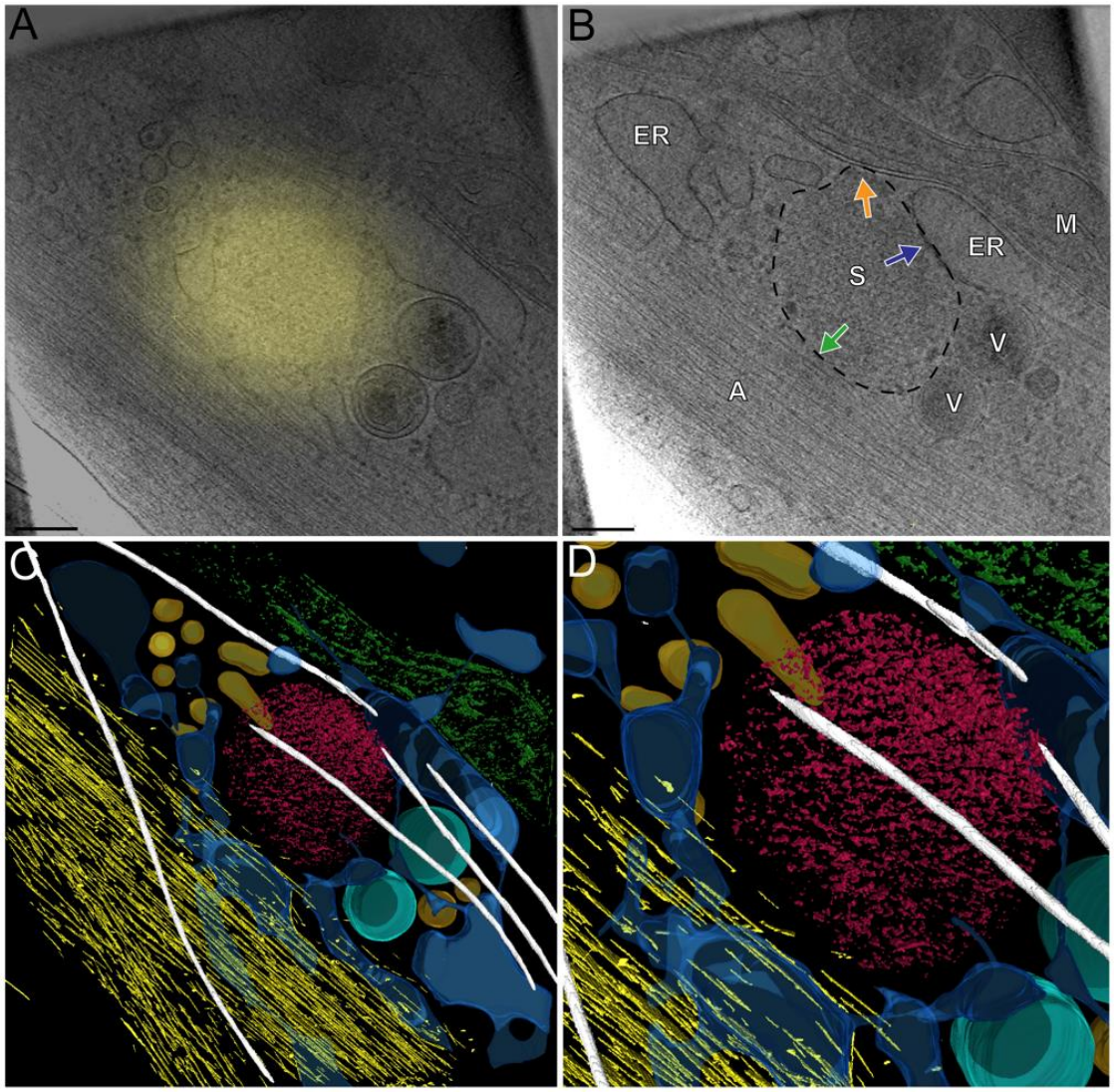

Supplementary figure 5. Carter et al

Figure S5. Cryo-CLEM reveals YFP-rhTRIM5α fluorescent bodies localize to cytosolic sequestosomes in association with actin filaments. (A) Cryo-CLEM signal of YFP-rhTRIM5α overlaid on a cryo-tomographic slice showing the corresponding location in an MG132-treated cell. **(B)** The same cryo-tomographic slice highlighting the border of the sequestosome with a black dashed line. The orange arrow highlights a mitochondrion/sequestosome in close proximity, the blue arrow highlights ER/sequestosome in close proximity, and the green arrow highlights an actin filament/sequestosome in close proximity. Scale bars = 200 nm. **(C)** 3D segmentation of the features in (B). **(D)** Enlarged view of the area of the sequestosome in (C).

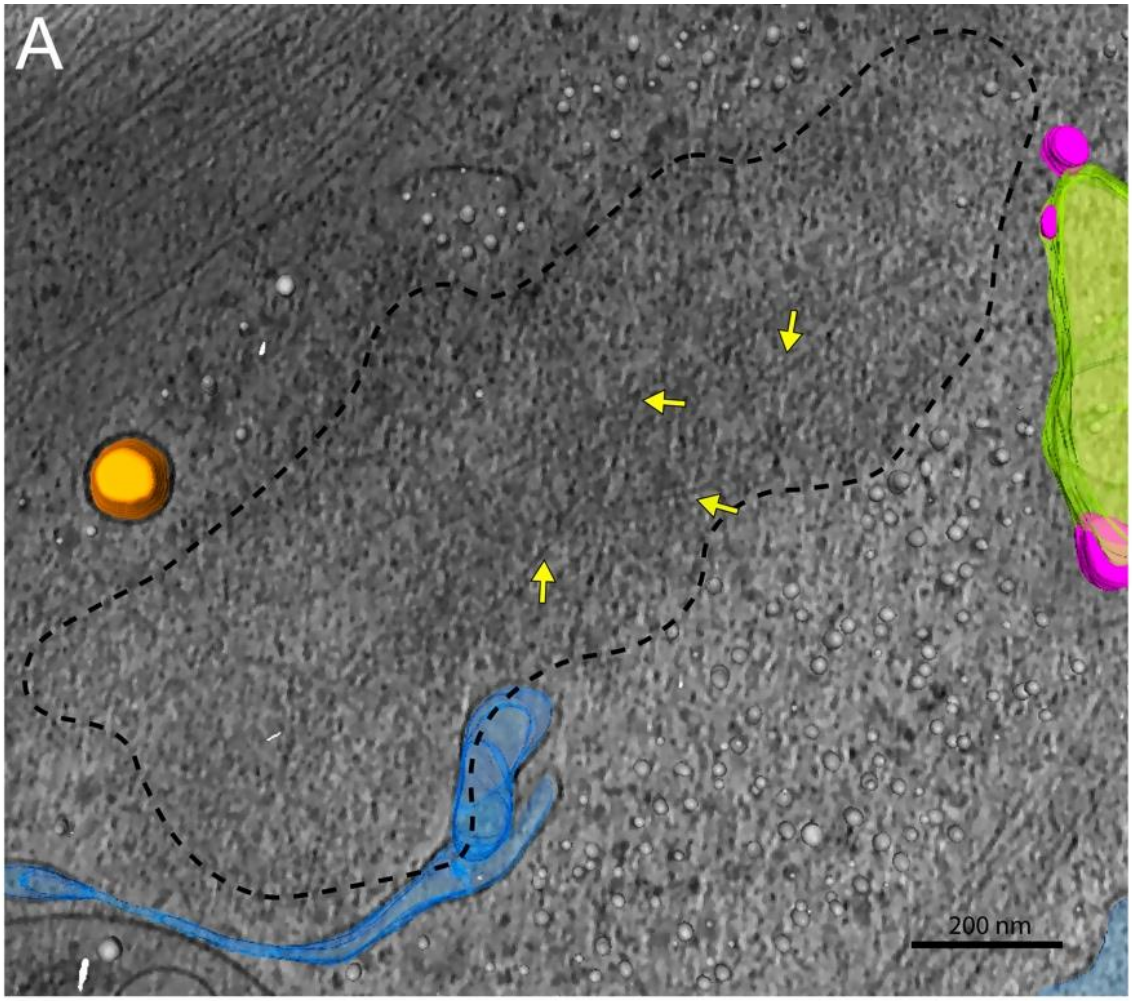

Supplementary figure 6. Carter et al

Figure S6. Actin filaments are observed inside sequestosomes. (A) A cryo-tomogram slice of a sequestosome outlined by black dashed line. Yellow arrows point to actin filaments. Scale bar = 200 nm.

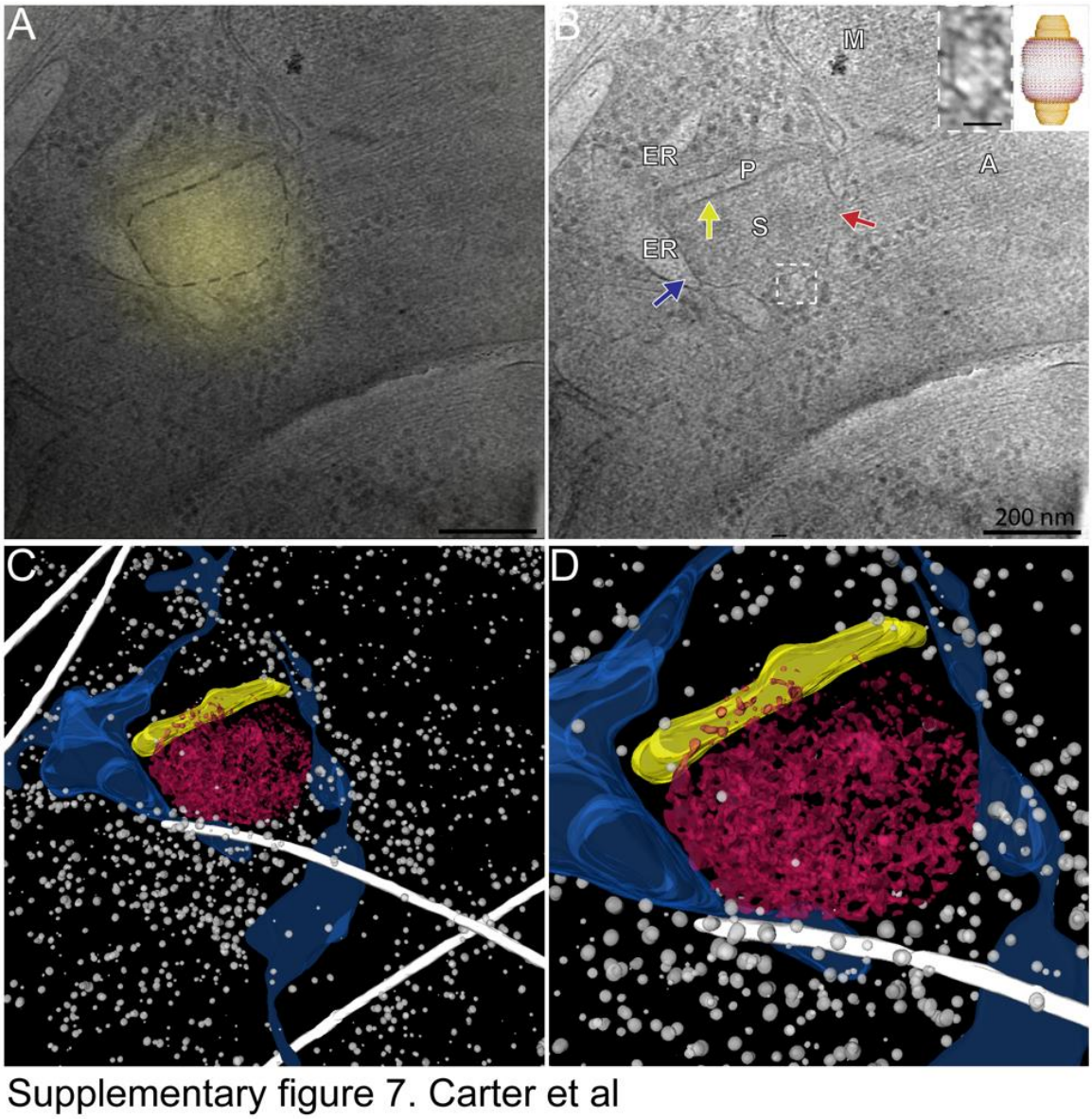

Figure S7. Cryo-CLEM reveals YFP-rhTRIM5α fluorescent bodies localized to a cytosolic sequestosome:phagophore complex. **(A)** Cryo-CLEM signal of YFP-rhTRIM5α overlaid on a cryo-tomographic slice showing the corresponding location in an untreated cell. **(B)** The same cryo-tomographic slice. The yellow arrow highlights a sequestosome:phagophore in close proximity, the red arrow highlights cytoplasm:sequestosome in close proximity, the blue arrow highlights an ER:sequestosome association. Scale bars = 200 nm. Inset shows an enlarged view of a vault from the region highlighted with a white dashed box, alongside the

crystal structure (PDB:4V60) of the vault complex. Scale bar = 20 nm. **(C)** 3D segmentation of the features in (B). **(D)** Enlarged view of the sequestosome:phagophore contact site in (C).

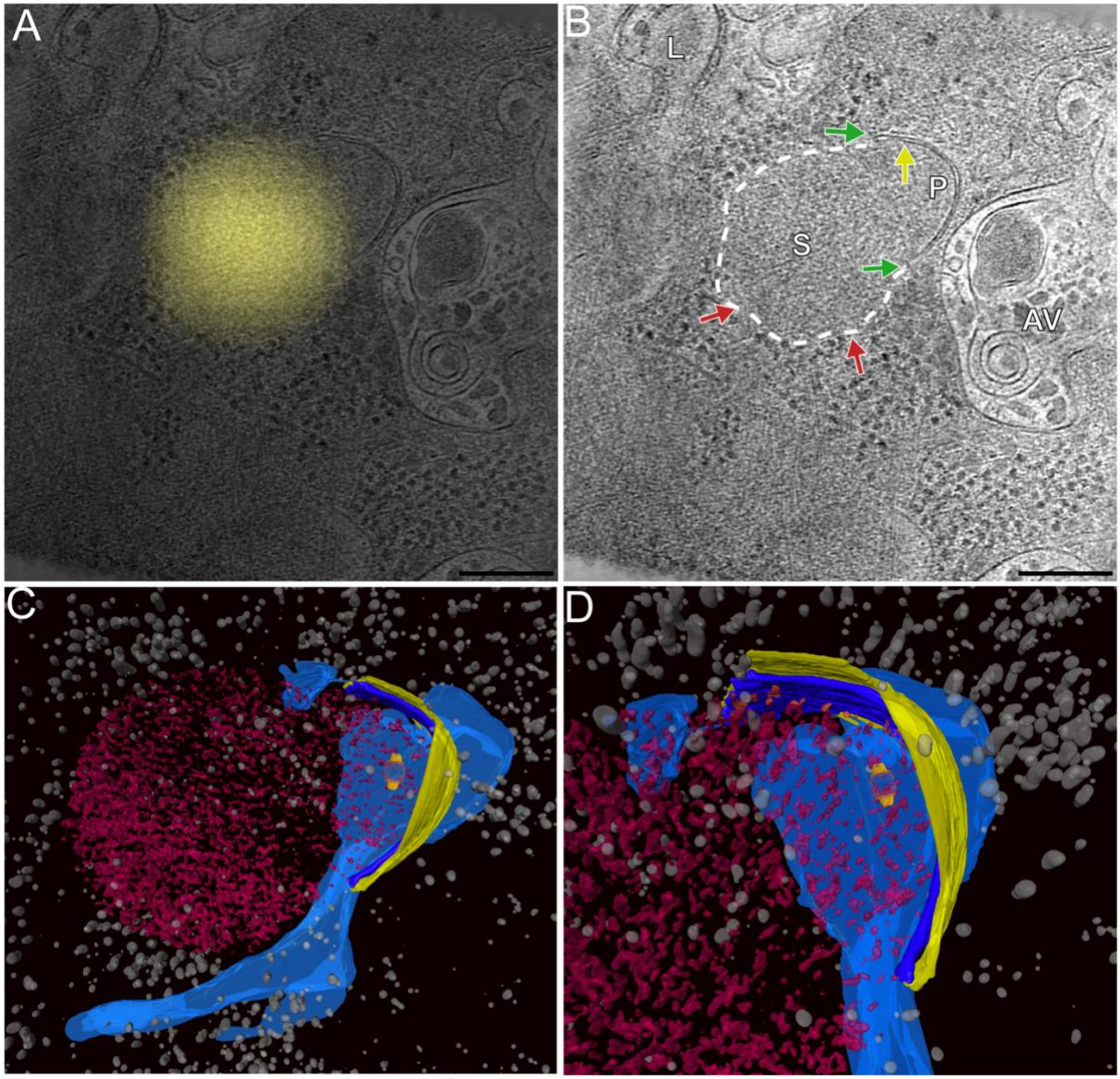

Supplementary figure 8. Carter et al

Figure S8. Cryo-CLEM reveals YFP-rhTRIM5α fluorescent bodies localized to a cytosolic sequestosome:phagophore complex in close association with the ER. **(A)** Cryo-CLEM signal of YFP-rhTRIM5α overlaid on a cryo-tomographic slice showing the corresponding location in an untreated cell. **(B)** The same cryo-tomographic slice, highlighting the border of the

sequestosome with a white dashed line. The yellow arrow highlights a sequestosome:phagophore in close proximity, the red arrows highlight cytoplasm:sequestosome in close proximity, and the green arrows highlight the extreme ends of the phagophore membrane. Scale bars = 200 nm. **(C)** 3D segmentation of the features in (B). **(D)** Enlarged view of the sequestosome:phagophore complex shown in (C).

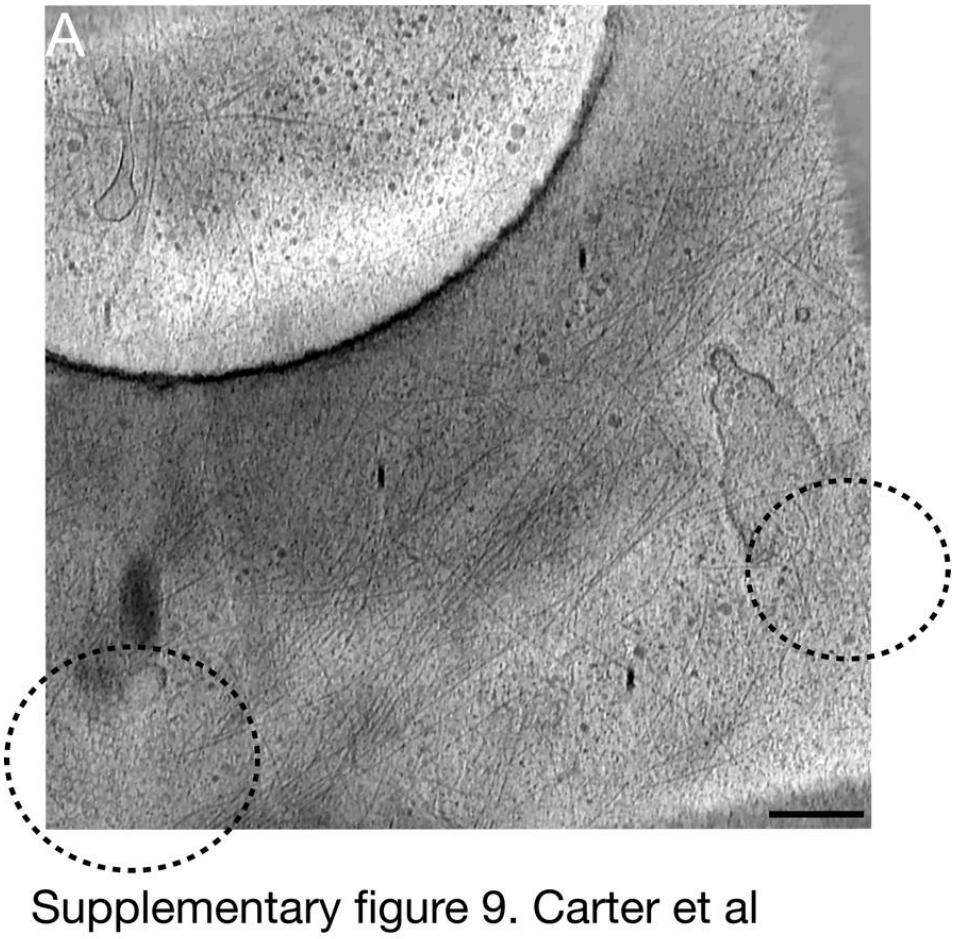

Figure S9. Hexagonal clathrin at the plasma membrane has nearly identical architecture to putative TRIM5α hexagonal nets found in the cytoplasm. **(A)** Cryo-tomographic slice showing hexagonal clathrin arrays at the plasma membrane, circled in black. Scale bar = 250 nm.

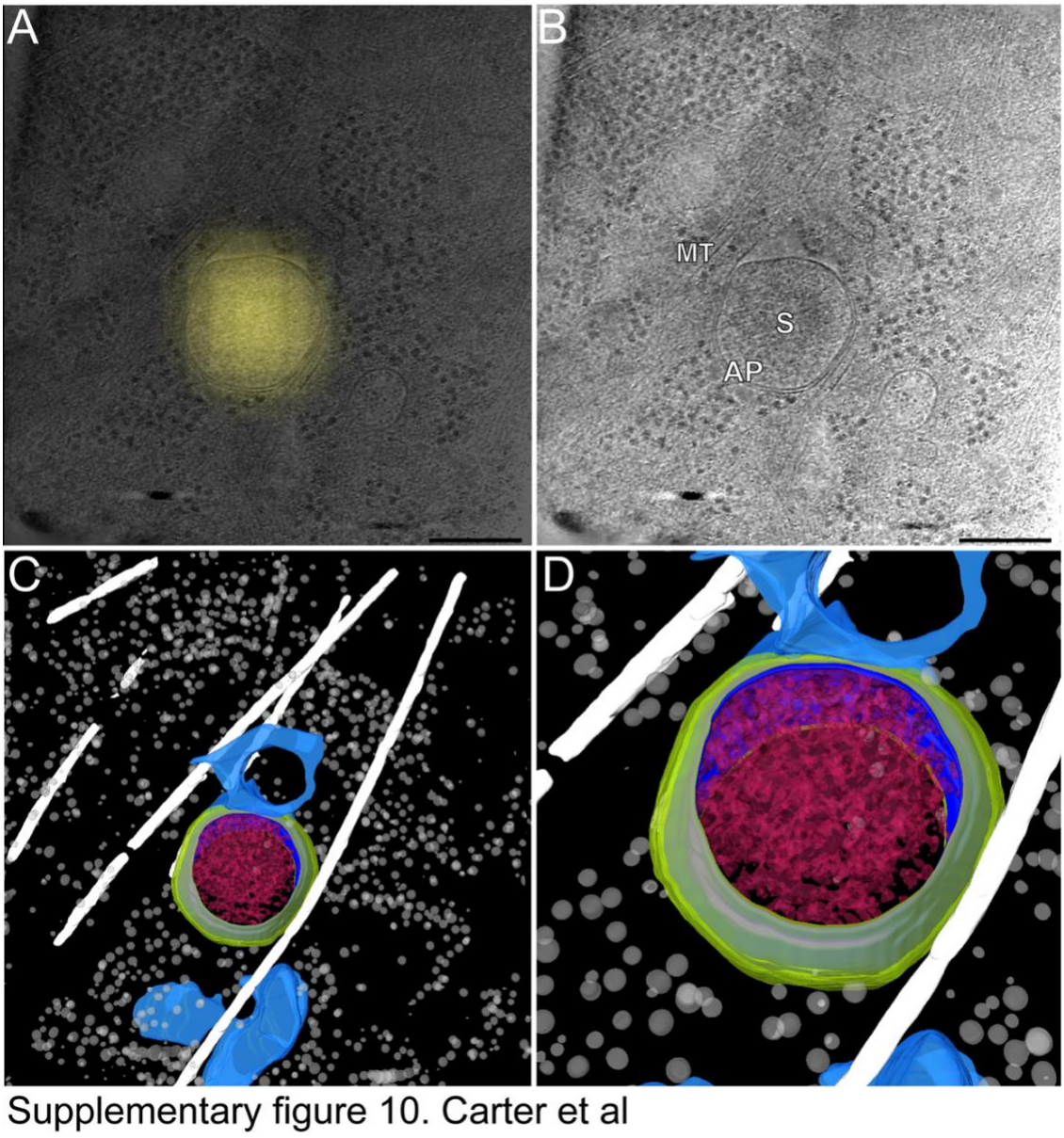

Figure S10. Cryo-CLEM reveals YFP-rhTRIM5α fluorescent bodies localized to an autophagosome. **(A)** Deconvolved epifluorescence image overlaid onto a high-magnification cryo-tomogram slice of an untreated cell. **(B)** The same cryo-tomographic slice without fluorescence, highlighting the sequestosome inside the autophagosome. Scale bars = 250 nm. **(C)** 3D segmentation of the features shown in (B). **(D)** Enlarged view of the enveloped sequestosome shown in (C).

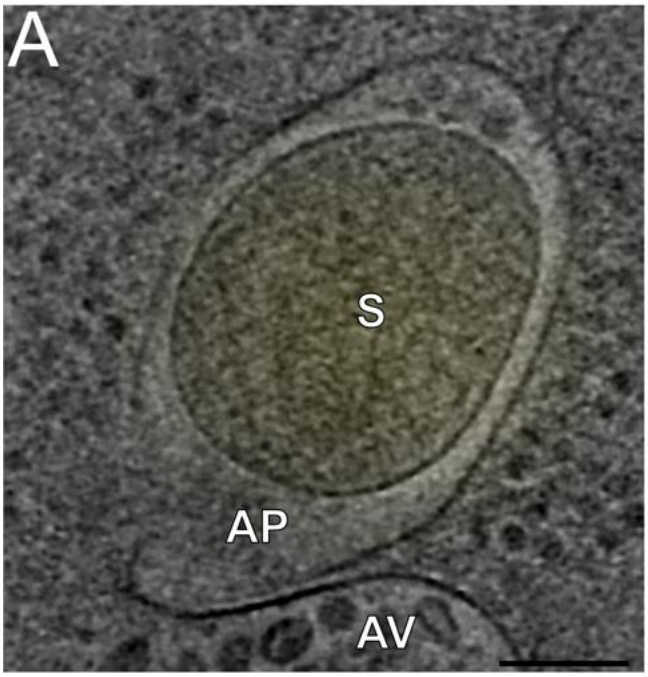

Supplementary figure 11. Carter et al

Figure S11. Cryo-CLEM reveals YFP-rhTRIM5α fluorescent bodies localized to an autophagosome. (A) Deconvolved epifluorescence image overlaid on a high-magnification cryo-tomogram slice of an untreated cell.

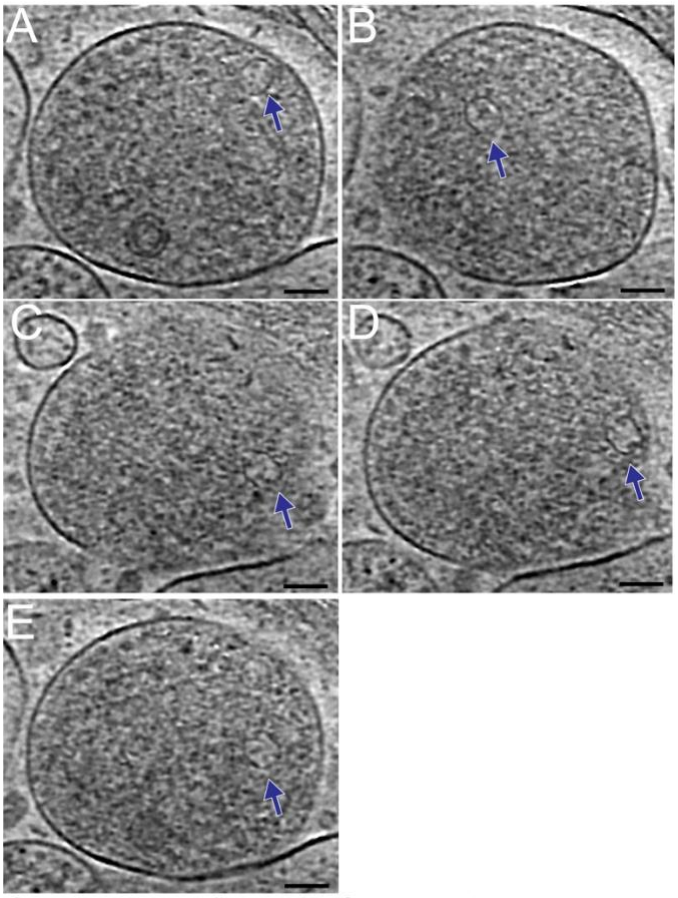

Supplementary figure 12. Carter et al

Figure S12. Vaults are found inside an autophagic vacuole. (A-E) Different cryo-tomographic slices of the autophagic vacuole shown in Figure 8. Blue arrows highlight 5 vaults within the inner lumen of a post-fusion autophagosome.

Reference

1. Tanaka, H. *et al.* The Structure of Rat Liver Vault at 3.5 Angstrom Resolution. *Science* **323**, 384–388 (2009).

Table S1. Table detailing previous reports of TRIM5α in proximity with other autophagy-related proteins.

Cell Type and Method	Interaction	Paper
293T Immunoprecipitation assay	TAK1, TAB2 and TAB3	Pertel et al. 2011
HeLa Fluorescence microscopy and Immunoprecipitation assay	p62	Mandell et al. 2014, O'Connor et al. 2010
HeLa cells Fluorescence microscopy	TRIM17	Mandell et al. 2014, Mandell et al. 2016
Coimmunoprecipitation X-ray crystallography Fluorescence microscopy	ATG8 paralogs - GABARAP GABARAPL1 LC3A, LC3B, LC3C and GABARAPL2	Mandell et al. 2014 Keown et al. 2018
HeLa cells Fluorescence microscopy	DFCP1 omegasome	Mandell et al. 2014
HeLa cells Fluorescence microscopy and 293T Coimmunoprecipitation assay	ULK1	Mandell et al. 2014
Proximity ligation assay	Beclin 1	Mandell et al. 2014
Immunoprecipitation assay	p62	Ribero et al. 2016
Immunoprecipitation assay	Atg16L1	Ribero et al. 2016
Immunoprecipitation assay	Atg5	Ribero et al. 2016

Table S2. Table detailing the cellular structures in this study that were imaged in cells untreated or treated with MG-132.

Cell	MG-132 Treatment	Cellular structure	Figure.	VPP
1	-	Sequestosome		No
1	-	2 x Autophagosome		No

2	-	Sequestosome	fig. S4 A and B	No
2	-	Phagophore		No
3	-	Autophagosome/Vaults	Fig. 7	No
3	-	Autophagic Vacuoles/Vaults	Fig. 8 and fig. S12	No
3	-	Phagophore/Sequestosome/Vault	fig. S7	No
4	-	Autophagosome	fig. S10	No
4	-	Autophagosome	fig. S11	No
5	-	Phagophore/TRIM5α 30 nm hexagons (net not extensive enough for clear Fourier transform)		No
6	-	Phagophore/Sequestosome/Vault	fig. S8	No
6	-	2 x Sequestosome		No
7	-	Autophagic Vacuoles		No
7	-	Vault	fig. S3	No
8	-	Autophagosome		No
9	+	2 x Autophagic Vacuoles		No
9	+	Phagophore/Hexagonal Net	Fig. 4	No
10	+	Phagophore/Sequestosome/Vault		No
11	+	Sequestosome	fig. S5	No
12	+	Autophagic Vacuoles		No
13	+	Sequestosome/Vaults	fig. S4 C-E	No
14	+	Sequestosome	Fig. 3 and fig. S6	No
15	+	Sequestosome		No
16	+	Sequestosome		No
17	+	Phagophore/Sequestosome		No
18	+	Sequestosome		No
19	+	Autophagosome		No
20	+	Vault	Fig. 2	No
21	+	Sequestosome		Yes
22	+	Sequestosome		Yes
22	+	Sequestosome		Yes
22	+	Sequestosome		Yes
23	+	Phagophore/Sequestosome/Hexagonal Net	Fig. 6	Yes
23	+	Sequestosome		Yes

24	+	Sequestosome		Yes
25	+	Sequestosome		Yes
26	+	Sequestosome		Yes

Table S2. Table detailing the cellular structures in this study that were imaged in cells untreated or treated with MG-132.

Movie Legends.

Movie S1. Movie illustrating the process of localizing YFP-rhTRIM5α to a sequestosome in HeLa cells by cryo-CLEM and cryo-ET. Low magnification (3,000x) cryo-EM images are correlated with epifluorescence images using clusters of 500 nm blue fluorospheres. Higher magnification cryo-tomograms are made transparent, overlaid and correlated with the low-magnification images. Finally, 3D isosurfaces are overlaid onto the cryo-tomogram.

Movie S2. Movie illustrating the process of localizing YFP-rhTRIM5α to a phagophore/hexagonal net in HeLa cells by cryo-CLEM and cryo-ET. Low magnification (3,000x) cryo-EM images are correlated with epifluorescence images using clusters of 500 nm blue fluorospheres. Higher magnification cryo-tomograms are made transparent, overlaid and correlated with the low-magnification images. Finally, 3D isosurfaces are overlaid onto the cryo-tomogram.

Movie S3. Movie showing the cryo-tomogram and isosurface of the sequestosome/phagophore complex shown in Fig. 6.

Movie S4. Movie showing the hexagonal net inside the phagophore in Fig. 6.

Movie S5. Movie showing the cryo-tomogram and isosurface of the autophagosome shown in Fig. 7.

Movie S6. Movie showing the inner portion of an autophagosome inside an autophagic vacuole. The lumen of this vesicle contains vaults highlighted in Fig. 8.

Movie S7. Movie showing the cryo-tomogram and isosurface of an isolated sequestosome shown in fig. S5.

Movie S8. Movie showing the cryo-tomogram and isosurface of the sequestosome/phagophore complex shown in fig. S7.

Movie S9. Movie showing the cryo-tomogram and isosurface of the sequestosome/phagophore complex shown in fig. S8.

Movie S10. Movie showing the cryo-tomogram and isosurface of the autophagosome shown in fig. S10.

Movie S11. Movie showing the cryo-tomogram of the autophagosome shown in fig. S11.